Galaxy Zoo: an independent look at the evolution of the bar fraction over the last eight billion years from *HST*-COSMOS[*]

Thomas Melvin,[1][†] Karen Masters,[1,2] Chris Lintott,[3] Robert C. Nichol,[1,2] Brooke Simmons,[3] Steven P. Bamford,[4] Kevin R. V. Casteels,[5] Edmond Cheung,[6] Edward M. Edmondson,[1] Lucy Fortson,[7] Kevin Schawinski,[8] Ramin A. Skibba,[9] Arfon M. Smith[10] and Kyle W. Willett[7]

[1]*Institute for Cosmology and Gravitation, University of Portsmouth, Dennis Sciama Building, Burnaby Road, Portsmouth PO1 3FX, UK*
[2]*SEPnet (South East Physics Network), www.sepnet.ac.uk*
[3]*Oxford Astrophysics, Department of Physics, University of Oxford, Denys Wilkinson Building, Keble Road, Oxford OX1 3RH, UK*
[4]*School of Physics and Astronomy, The University of Nottingham, University Park, Nottingham NG7 2RD, UK*
[5]*Institut de Cincies del Cosmos. Universitat de Barcelona (UB-IEEC), Mart i Franqus 1, E-08028 Barcelona, Spain*
[6]*Department of Astronomy and Astrophysics, 1156 High Street, University of California, Santa Cruz, CA 95064, USA*
[7]*School of Physics and Astronomy, University of Minnesota, Minneapolis, MN 55455, USA*
[8]*Department of Physics, Institute for Astronomy, ETH Zurich, Wolfgang-Pauli-Strasse 27, CH-8093 Zurich, Switzerland*
[9]*Center for Astrophysics and Space Sciences, Department of Physics, University of California, 9500 Gilman Dr., San Diego, CA 92093, USA*
[10]*Adler Planetarium, 1300 S Lake Shore Drive, Chicago, IL 60605, USA*

ABSTRACT

We measure the redshift evolution of the bar fraction in a sample of 2380 visually selected disc galaxies found in Cosmic Evolution Survey (COSMOS) *Hubble Space Telescope* (*HST*) images. The visual classifications used both to identify the disc sample and to indicate the presence of stellar bars were provided by citizen scientists via the Galaxy Zoo: Hubble (GZH) project. We find that the overall bar fraction decreases by a factor of 2, from 22 ± 5 per cent at $z = 0.4$ ($t_{lb} = 4.2$ Gyr) to 11 ± 2 per cent at $z = 1.0$ ($t_{lb} = 7.8$ Gyr), consistent with previous analysis. We show that this decrease, of the strong bar fraction in a volume limited sample of massive disc galaxies [stellar mass limit of $\log(M_\star/M_\odot) \geq 10.0$], cannot be due to redshift-dependent biases hiding either bars or disc galaxies at higher redshifts. Splitting our sample into three bins of mass we find that the decrease in bar fraction is most prominent in the highest mass bin, while the lower mass discs in our sample show a more modest evolution. We also include a sample of 98 red disc galaxies. These galaxies have a high bar fraction (45 ± 5 per cent), and are missing from other COSMOS samples which used SED fitting or colours to identify high-redshift discs. Our results are consistent with a picture in which the evolution of massive disc galaxies begins to be affected by slow (secular) internal process at $z \sim 1$. We discuss possible connections of the decrease in bar fraction to the redshift, including the growth of stable disc galaxies, mass evolution of the gas content in disc galaxies, as well as the mass-dependent effects of tidal interactions.

Key words: galaxies: evolution – galaxies: spiral – galaxies: structure.

1 INTRODUCTION

A variety of physical processes act to change the morphologies of galaxies over their lifetimes, from being hot, clumpy and floccu-

lent in the high-redshift Universe (Elmegreen et al. 2009), to dynamically cool, disc-dominated spiral galaxies (Weiner et al. 2006; Kassin et al. 2007; Sheth et al. 2012) and, in some cases, to lenticular or elliptical galaxies in the local Universe. These processes are either external or internal to the galaxy in question. External processes are dominated by dramatic, dynamically fast processes, such as galaxy–galaxy interactions. Mergers, both major and minor, rapidly change the morphology of a galaxy, with this violent phase of galaxy evolution being dominant at higher redshifts (e.g. Abraham 1999; Ryan et al. 2008; Lin et al. 2008; Kartaltepe et al. 2010;

Lotz et al. 2011). As the Universe expands and the galaxy population becomes more mature, major mergers become rare in all but the densest parts of the Universe. The major merger rate is also dependent on the stellar masses of the galaxies involved (e.g. Conselice et al. 2003; Conselice, Rajgor & Myers 2008). For example, the last major merger for our Milky Way, a relatively massive disc galaxy, was believed to have been 10–12 Gyr ago (Wyse 2001; Gilmore, Wyse & Norris 2002).

In this era, slower and often internally driven processes become more important to the evolution of galaxies. These processes are often dependent on the host galaxy's properties, e.g. the shape of its dark matter halo, its stellar mass or its gas content (see Sellwood 2013 and references therein for examples). This calmer period of evolution affects the evolution of massive, well-formed disc galaxies in the local Universe and is often referred to as the 'secular epoch'. In this paper we focus on studying the cosmic evolution of one of the major drivers of secular evolution in disc galaxies: the formation and evolution of barred stellar structures since $z = 1$.

Bars form naturally in dynamically cool disc galaxies, stabilizing stellar orbits by allowing gas to dissipate energy and fall inwards towards the galactic centre, while the angular momentum is redistributed to both the stellar and dark matter halo (e.g. Athanassoula 2005, 2012; Combes 2009). This is one of many influences a bar has on its host galaxy, and determining which other morphological and physical properties are directly affected by the presence of a bar is of significant interest to the understanding of how galaxy populations are evolving in the secular epoch.

Theoretical understanding of the impact of bar formation on galactic discs, along with observational studies, suggests that the possible evolutionary effects of bars include: (i) the formation of a pseudo-bulge at the galaxy's centre (Pfenniger & Norman 1990; Kormendy & Kennicutt 2004; Combes 2009; Athanassoula 2012), (ii) the fuelling of star formation at the galaxy's centre (Sérsic & Pastoriza 1965; Hawarden et al. 1986; Ho, Filippenko & Sargent 1997; Martinet & Friedli 1997; Sakamoto et al. 1999; Sheth et al. 2005; Ellison et al. 2011), (iii) possible feeding of a central active galactic nucleus (Knapen, Shlosman & Peletier 2000; Coelho & Gadotti 2011; Oh, Oh & Yi 2012; Alonso, Coldwell & Lambas 2013), although no correlation between active galactic nuclei activity and bar fraction has been observed so far (Mulchaey & Regan 1997; Regan & Mulchaey 1999; Cisternas et al. 2013); (iv) a possible role in the cessation of star formation, thereby moving the galaxy on to the red sequence (Masters et al. 2010, 2012; Saintonge et al. 2012; Wang et al. 2012; Cheung et al. 2013). The overall conclusion from these, and other works, is that bars do play an important role in the evolution of disc galaxies in the local Universe (although for an opposing view see van den Bergh 2011 and references therein).

Many observations have been made to determine the quantity of stellar bars in our local Universe ($z < 0.1$). The abundance of bars can be quantified as the bar fraction (f_{bar}), which is simply found by calculating what fraction of disc galaxies in a sample possess a barred structure. In the local Universe, observed bar fractions range from 25 to 70 per cent depending on several selection effects: (i) bar classification method, (ii) the strength of the bars observed, (iii) which wave-bands they are observed in. The selection of discs can also affect the outcome, with the denominator of the bar fraction being dependent on whether S0s, S0/as or Sdms are included as disc galaxies.

The high resolution of the *Hubble Space Telescope* (*HST*) allowed astronomers to begin exploring the bar fraction at higher redshifts. Small samples of disc galaxies from early *HST* observations found conflicting results as to how the bar fraction evolved towards higher redshifts. Abraham et al. (1999) found a decreasing bar fraction towards higher redshifts, while Elmegreen, Elmegreen & Hirst (2004) and Jogee et al. (2004) observed a constant bar fraction up $z \sim 1$. Sheth et al. (2003, 2004) also observed a constant bar fraction towards higher redshifts, but this was for only the largest bars, due to the coarse resolution of the NICMOS camera. Using a sample of disc galaxies an order of magnitude larger ($\approx$2000) than any previous study, Sheth et al. (2008) [hereafter S08] presented a result where the bar fraction declined towards higher redshifts (across the range $0.2 < z < 0.84$). This result has since been replicated by Cameron et al. (2010), who explored the trend using a sample of $\sim$900 disc galaxies across the redshift range $0.2 < z < 0.6$. It is also worth noting that, in light of these more recent works, the trends presented by Elmegreen et al. (2004) and Jogee et al. (2004) can also be interpreted as a declining bar fraction towards higher redshifts.

Understanding whether the bar fraction evolves across cosmic time-scales is important. Typically, bars tend to form in galaxies which have become relaxed, cool and disc dominated, although it is worth noting that some bars may also be formed by galaxy–galaxy interactions (Barnes & Hernquist 1991; Cox et al. 2008; Hopkins et al. 2009). Although these interactions can also destroy bars, they are typically long lived features, and so the presence of a barred structure can be used as a tracer for when disc galaxies become dynamically stable and 'mature'. Once a disc galaxy reaches this dynamically relaxed state, in the absence of external influences, secular processes begin to dominate its evolution.

Here, we complement and expand on the work of S08, with our observations exploring the redshift evolution of the bar fraction over a wider range of redshifts, and extending to higher redshifts ($0.4 \leq z \leq 1.0$), as well as exploring its dependence on stellar mass [$\log (M_\star/M_\odot) > 10.0$]. As in both S08 and Cameron et al. (2010), we base our study on images taken as part of the Cosmic Evolution Survey (COSMOS; Scoville et al. 2007b); however we use a different sample selection and bar identification method (see Section 2 for more details). We combine photometric and spectroscopic data from COSMOS with visual morphological classifications from the third incarnation of the Galaxy Zoo project,[1] namely the Galaxy Zoo: Hubble (GZH)[2] project, producing a catalogue of 2380 disc galaxies (317 barred). Using these visual classifications allows us to include a sample of quiescent disc galaxies in our work.

In Section 2 we describe the selection criteria used to produce our disc galaxy sample, including how GZH classifications are used. In Section 3 we explore potential biases in our sample. We present our results in Section 4, followed by a discussion in Section 5. Finally, we finish with our summary and conclusions in Section 6. Throughout this paper we use the AB magnitude system, and where necessary we adopt the following cosmology; $H_0 = 70 \, \mathrm{km \, s^{-1} \, Mpc^{-1}}$, $\Omega_m = 0.28$ and $\Omega_\Lambda = 0.72$ (Bennett et al. 2012).

2 DATA AND SAMPLE

2.1 COSMOS

We provide a brief summary of the observational photometric and spectroscopic data obtained by COSMOS and the selection criteria we apply. A more detailed discussion of COSMOS and the *HST* imaging can be found in Scoville et al. (2007a,b).

[1] www.galaxyzoo.org

[2] hubble.galaxyzoo.org

The COSMOS survey observed galaxies using the *HST* Advanced Camera for Surveys (ACS) F814W (*I*-band) filter over a 2 deg^2 equatorial field. With its excellent spatial resolution (0.05 arcsec pixel^{-1}), the ACS is able to observe structures with radii smaller than 1 kpc up to redshifts of $z = 1$. This resolution is ideal for detecting galactic bars, whose typical lengths in the local Universe are in excess of 2 kpc (Elmegreen & Elmegreen 1985; Barazza, Jogee & Marinova 2008; Aguerri, Méndez-Abreu & Corsini 2009; Hoyle et al. 2011) (also see Menéndez-Delmestre et al. 2007; Sheth et al. 2003 and section 2 of S08 for an alternative discussion of bar resolution using the ACS). Initial ACS observations were followed up with observations from a wide range of telescopes, which provided additional data across 16–30 different wave-bands for each galaxy (Capak et al. 2007; Scoville et al. 2007b; Ilbert et al. 2009).

In addition to the imaging, a follow-up spectroscopic survey (zCOSMOS; Lilly et al. 2007, 2009) provided spectroscopic redshifts for a fraction of galaxies detected in COSMOS (12 per cent of Galaxy Zoo COSMOS galaxies are included). The remaining galaxies have photometric redshifts taken from Ilbert et al. (2009). For detailed discussions of the spectroscopic and photometric redshifts used in this paper, see Lilly et al. (2007) and Ilbert et al. (2009) respectively, while Griffith et al. (2012) provide a useful summary of this information for the COSMOS galaxies used in GZH (see section 2.3.2 of Griffith et al. 2012).

We apply the redshift range $0.4 \leq z \leq 1.0$ to our COSMOS galaxies. The lower limit is chosen so that the *HST* imaging resolves structures of similar size to those observed in the Sloan Digital Sky Survey (SDSS) Main Galaxy Sample (Strauss et al. 2002) at $z \sim 0.1$ (see Section 2.3). We note that SDSS imaging can resolve structures on scales of 2.2 kpc at $z = 0.04$ (approximately the mid-redshift point of the low-redshift sample; see Section 2.3), while the ACS minimum resolution ranges from 1.3 kpc at $z = 0.4$ to 2 kpc at $z = 1$. Therefore, despite large differences in angular resolutions, the surveys are well matched in physical resolution and are able to observe all large-scale barred structures in their respective redshift ranges.

The upper redshift limit is set not by the constraints of resolution, but by band shifting. Fig. 1 highlights this effect on the ACS F814W filter, showing it shifting bluewards across the rest-frame SDSS *ugriz* filters as the redshift increases. Identification of bars in the bluest and/or UV wavelengths is known to be hampered by the effects of clumpy star formation hiding the smooth bar structure, with bars also becoming dimmer in these bands due to being dominated by older stellar populations. S08 demonstrated this effect, showing a reduction in bar identification in the SDSS *u*-band filter relative to the *griz* filters (see their fig. 7 in Appendix A1; this was especially a problem when using an ellipse fitting method to identify bars). In this study we do begin to probe the rest-frame *u* band, but even at our highest redshift ($z = 1$), 52 per cent of the light gathered in the F814W band is above the 4000 Å break (bars become difficult to detect bluewards of this break). Therefore, despite partly probing the rest-frame *u* band, we are still predominantly probing the rest-frame *g* band, where there is no depreciation in bar detection. We expect to detect all strong bars that are present within the full redshift range we explore ($0.4 \leq z \leq 1.0$), but if we exclude galaxies at $z > 0.84$, our main conclusions are unaffected.

In addition, we apply the following stellar mass limit to our data: $\log(M_\star/M_\odot) \geq 10$, as shown in Fig. 2. Although we apply the same mass limit at all redshifts, this is consistent with exploring disc galaxies from the same area of the stellar mass function distribution at all redshifts, as $M_\ast$ does not evolve significantly across the redshifts we explore (Bundy et al. 2006; Ilbert et al. 2010, 2013).
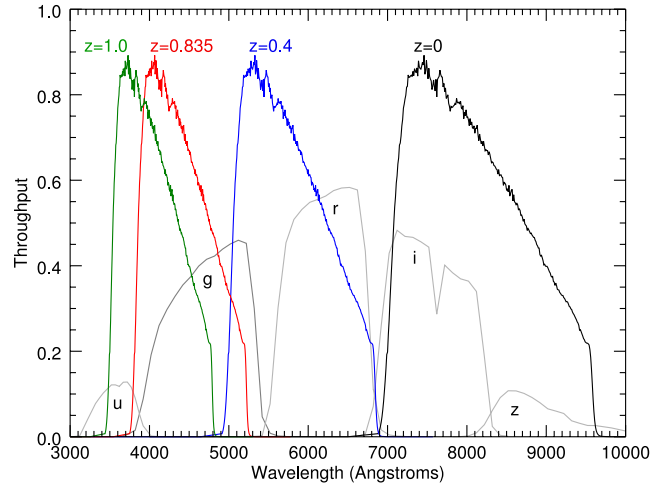
Figure 1. Band shifting effects of the ACS F814W (*I*-band) filter across the rest-frame SDSS *ugriz* filters (grey). The F814W filter is traced from $z = 0$ (black) through to $z = 1.0$ (green). We also show the lower redshift limit of our sample (blue) and the upper limit applied in S08 (red). All filters shown use throughput values with atmosphere, optics and detector effects included. This figure is based on fig. 8 of S08 and is reproduced here for the benefit of the reader.
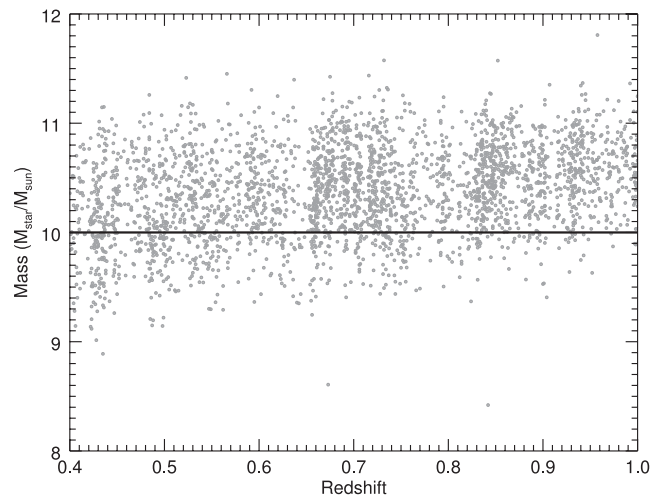

Figure 2. Distribution of stellar masses versus redshift for all visually classified face-on disc galaxies imaged by COSMOS over the redshift range $0.4 \leq z \leq 1.0$. Bold horizontal line shows the mass limit [$\log(M_\star/M_\odot) \geq 10.0$] applied to the main sample selection.

The stellar mass estimates used here are taken from Mobasher et al. (2007), with an expected error less than 0.5 dex (see section 6.1 of Mobasher et al. 2007 for details of the stellar masses used in this paper). We also note that these stellar masses are the same as those used in S08. The mass limit is applied so that the low-mass galaxies explored are detectable across the whole redshift range.

2.2 Galaxy Zoo: Hubble

Running from 2010 April 23 until 2012 September 10, Galaxy Zoo: Hubble (hereafter GZH) was the third incarnation of the Galaxy Zoo project (GZ), and the first to show images from the *HST*. During this time, GZH attracted 86 520 individual volunteers who in turn provided 40 631 068 individual clicks.
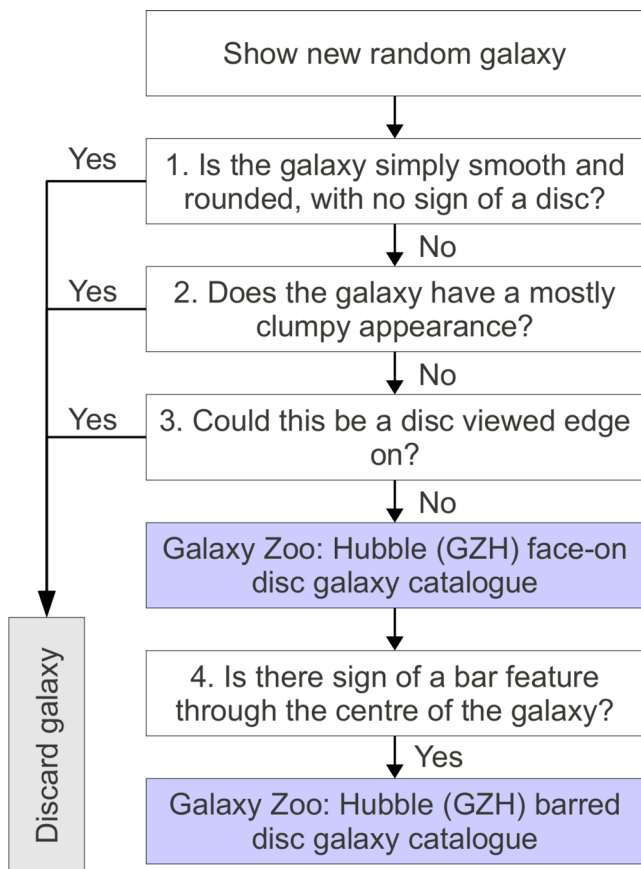
Figure 3. Edited GZH decision tree.[3] Questions shown are relevant to producing the GZH disc and barred disc samples.

To classify a galaxy, a volunteer is first shown a randomly selected image of a galaxy and is asked; (1) *is the galaxy simply smooth and rounded with no sign of a disc?* Their answer to this question determines any further questions they are asked about each galaxy, with the GZH decision tree used in this work being an updated version of the decision tree used in Galaxy Zoo 2 (Willett et al. 2013, hereafter W13). We show an edited version of the GZH decision tree,[3] in Fig. 3, which shows that a volunteer who answers 'no' to questions 1–3 (as numbered in Fig. 3) classifies a galaxy as being a face-on disc galaxy. Furthermore, a volunteer who answers question 4 with 'yes' classifies said galaxy as barred.

As each galaxy is viewed by many volunteers (the minimum number of volunteers that classify a galaxy is 33, with the median number of volunteers being 47), the clicks provided by each volunteer are combined with those made by other volunteers to produce morphological classifications for each galaxy which are represented by 'vote fractions', i.e. the fraction of volunteers answering a given question positively. These vote fractions, or estimated likelihoods (p), are constructed via a weighting scheme where volunteers whose individual classifications tend to disagree with the majority are downweighted. This weighting rewards consistency and removes outliers. An in-depth discussion of the original GZ project, including how volunteers' classifications are weighted and combined, is provided in Lintott et al. (2008), the appendix of Bamford et al.

(2009) and Lintott et al. (2011). This method was repeated for GZ2 in W13, with similar methods applied to the GZH classifications.

To determine whether a galaxy is a face-on disc, we apply a minimum threshold of $p \geq 0.5$ for questions 1–3 (Fig. 3). In explicit terms, we require the following: $p_{\text{not-smooth}} \geq 0.5$; $p_{\text{not-clumpy}} \geq 0.5$; $p_{\text{not-edgeon}} \geq 0.5$. The threshold chosen ($p \geq 0.5$) for each of the questions posed is a compromise between the sample size and its purity. A higher threshold (say $p \geq 0.7$) would offer a purer but smaller sample. Conversely, a lower threshold (say $p \geq 0.3$) would increase the sample size, but at the expense of including more uncertain classifications. In addition to our threshold criteria, we apply an inclination cut similar to those used in other studies of bars [$\log(a/b) \leq 0.3$],[4] as well as removing any galaxies that are obviously merging ($p_{\text{merger}} \geq 0.65$ with a minimum of 18 volunteers answering the *Is there anything odd?* question). This produces the final sample size of 2,380 face-on disc galaxies. Hereafter, our face-on disc sample is referred to as our 'GZH sample'.

Finally, to classify a GZH disc galaxy as barred, we apply the same threshold used in questions 1–3 to question 4; $p_{\text{bar}} \geq 0.5$, with a median of 29 volunteers having answered question 4. This criterion gives a sample of 317 barred disc galaxies ($f_{\text{bar}} = 13.3 \pm 0.7$ per cent for whole sample), which will be referred to as our 'barred GZH sample' herein. A selection of images of the GZH and barred GZH samples are shown in Fig. 4.[5] We explore the effects of using different thresholds in Appendix A1, finding that they vary the absolute value of the bar fraction at all redshifts, but do not significantly change the trends we observe. Additionally, when exploring lower thresholds for $p_{\text{not-smooth}}$, the trend we observe remains robust.

2.3 Local comparison sample

We make use of a low-redshift sample of disc galaxies as a comparison set for our GZH sample. We use classifications from Galaxy Zoo 2 (GZ2)[6] (W13), specifically the GZ2 disc sample, which was used to explore trends of the bar fraction with galaxy properties in our local Universe (Masters et al. 2011, 2012, hereafter M12). Here, we use the revised sample from M12, which was based on the final GZ2 classifications. We briefly discuss how this sample was compiled; a more detailed description can be found in Masters et al. (2011) and M12.
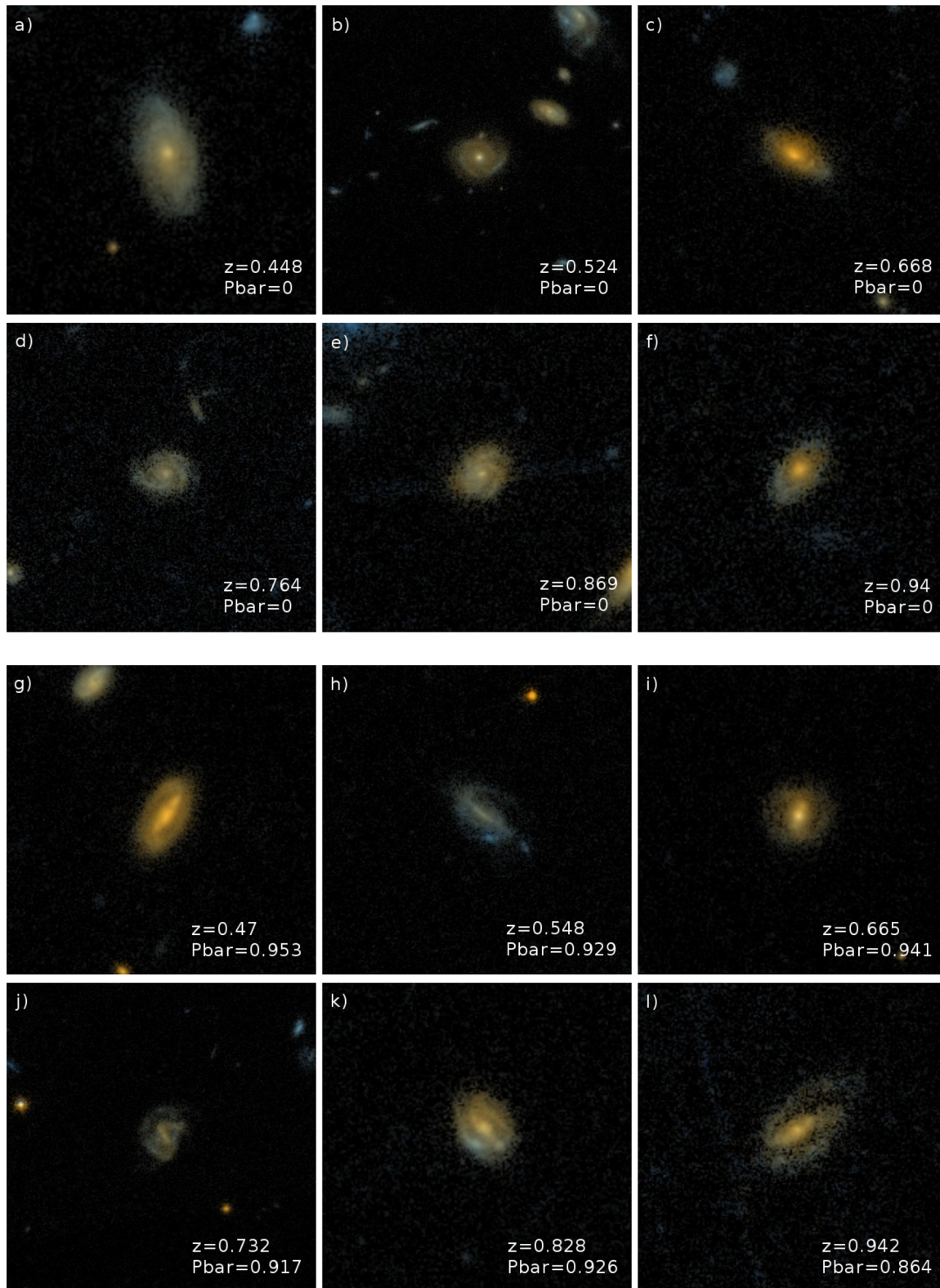
The GZ2 disc galaxy catalogue is based on bright ($r < 17$) galaxies from the SDSS Main Galaxy Sample (Strauss et al. 2002). These were used in the second GZ phase that ran from 2009 to 2010. A volume limit ($0.017 < z < 0.06$; $M_r < -20.15$) was applied, as well as an inclination cut [$\log(a/b) < 0.3$]. Each of these galaxies was visually classified in GZ2, with a median number of 45 independent classifiers for each galaxy. The decision tree used in GZ2 to determine the disc galaxy sample is similar to that used for the GZH sample, with the main difference relevant to this study being the omission of the question: '*does the galaxy have a mostly clumpy appearance?*'. M12 applied a threshold of $p \geq 0.5$ for each question to define the face-on disc and barred disc galaxies. This produced a final sample of 15 292 disc galaxies (GZ2 sample hereafter), with an overall bar fraction of 26.2 ± 0.4 per cent.

---

[4] Semi-major and semi-minor axis are measured using SEXTRACTOR and are taken from the COSMOS 2005 morphology catalogue – http://irsa.ipac.caltech.edu/data/COSMOS/datasets.html

[5] Images of the full sample are available at http://data.galaxyzoo.org/.

[6] http://zoo2.galaxyzoo.org/

[3] The full GZH decision tree can be seen at http://data.galaxyzoo.org

Figure 4. Postage stamp images showing six unbarred galaxies from our GZH sample (images $a - f$) and six barred galaxies from our GZH sample (images $g - l$). The images are organized in ascending redshifts for each sample, with the redshift and weighted estimated likelihood from GZ classifications that the galaxy hosts a barred structure (p_{bar}) shown in the bottom right hand corner. These are images taken by ACS in the F814W band, with additional Subaru B_J, r^+ and i^+ images added to produce the pseudo-colour images shown (Griffith et al. 2012). See Fig. A1 for examples at intermediate p_{bar} values.

M12 compared the GZ2 classifications with those from Nair & Abraham (2010). Using a cross-matched sample of 3638 disc galaxies, M12 conclude that disc galaxies with a $p_{bar} \geq 0.5$ (as used in Masters et al. 2011, and M12) corresponded to strong bar classifications made by Nair & Abraham (2010). M12 also found reasonable agreements with strong bar classifications made by de Vaucouleurs et al. (1991) and Barazza et al. (2008). Similarly, when comparing GZ2 bar classifications with those made by the Extractions de Formes Idéalisées de Galaxies en Imageriem (EFIGI) group (Baillard et al. 2011), W13 conclude that GZ2 classifications are excellent for identifying strong bars in disc galaxies, but may miss shorter bars.

We use these comparisons, along with the fact that the physical resolution of the *HST* and SDSS images are comparable within their respective redshift ranges, to argue that our selection of $p_{bar} \geq 0.5$ from GZH classifications may be interpreted as an identification of a strong bar in the observed galaxy. Here we describe a strong bar as being one which is easily identifiable in its host galaxy.

Here, we carefully review the make-up of our GZH and GZ2 disc samples to avoid confusion with comparisons with other disc, spiral or late-type selections based on GZ morphologies. The disc galaxy selections presented herein possibly include a fraction of early-type disc galaxies (Sa or S0), which would normally be included in a majority of early-type samples selected by either colour or central concentration. This results in our diverse disc galaxy samples showing bimodality in their optical colour magnitude. However, other GZ samples which were more focused on late-type discs or spiral galaxies (Sb, Sc or later) can be constructed using the Galaxy Zoo 1 'clean' spiral criterion, as first discussed in Land et al. (2008), and most recently used in Schawinski et al. (2013). This can also be achieved by applying stricter limits in GZ2/GZH data. This more conservative late-type sample will be more dominated by 'blue cloud' spirals and thus show less bimodality of their galaxy properties.
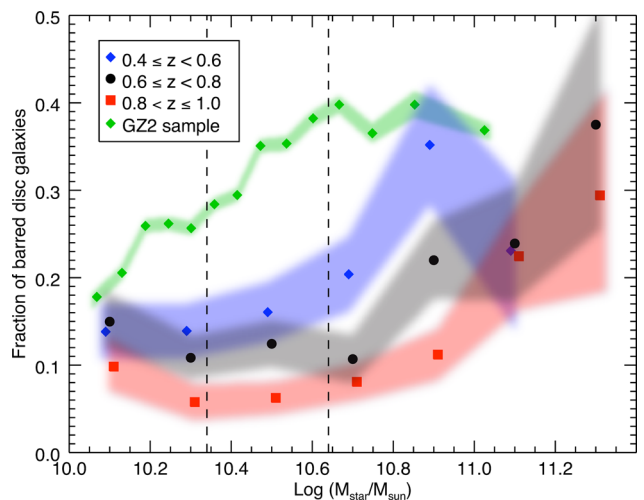
2.4 Stellar mass subsamples

It is now understood that the bar fraction in disc galaxies depends on the stellar mass distribution of the sample (e.g. Nair & Abraham 2010). Fig. 5 shows the dependence of bar fraction on stellar mass for our GZH sample across three redshift bins: $0.4 \leq z < 0.6$ (blue); $0.6 \leq z < 0.8$ (black); $0.8 \leq z \leq 1.0$ (red). We also include $z \sim 0.1$ data from the GZ2 sample (green). In each of the GZH redshift bins we observe increasing bar fractions towards higher stellar masses, with this trend also seen in the GZ2 sample.

We split the GZH (and GZ2) sample into three stellar mass subsamples, each containing approximately the same number of galaxies. These mass cuts are shown as vertical dashed lines in Fig. 5. In detail, the subsamples are:

1. Low mass: Galaxies having stellar masses, $10.0 \leq \log(M_\star/M_\odot) < 10.34$. For the GZH sample this contains 789 disc galaxies (3782 in the GZ2 sample).

2. Intermediate mass: Galaxies having stellar masses $10.34 \leq \log(M_\star/M_\odot) < 10.64$, which represents the typical transitional mass between the blue cloud and red sequence in the local Universe (Kauffmann et al. 2003; Baldry et al. 2004). For the GZH sample this contains 801 disc galaxies (4384 in the GZ2 sample).

3. High mass: Galaxies with masses $\log(M_\star/M_\odot) \geq 10.64$. In the local Universe disc galaxies with these masses are significantly more likely to be found on the red sequence (e.g. Masters et al.

Figure 5. Bar fraction versus stellar mass for three redshift bins: $0.4 \leq z < 0.6$ (blue), $0.6 \leq z < 0.8$ (black) and $0.8 \leq z \leq 1.0$ (red). We also show the GZ2 disc galaxy sample (green). Vertical dashed lines show the mass limits that define our three GZH subsamples.

2010). For the GZH sample this contains 790 disc galaxies (2995 in the GZ2 sample).

We note that at typical star formation rates (SFR) of 1–2 $M_\odot$ yr^{-1} (at $z = 1$) a disc galaxy could gain extra stellar mass totalling up to $\sim 10^{10} M_\odot$ over the 8 Gyr from $z = 1$ to $z \sim 0$. This could move some of the lowest mass galaxies at $z \sim 1$ into the intermediate-mass bin by $z \sim 0$, as well as moving some of the intermediate-mass galaxies into the high-mass bin by $z \sim 0$. However, this mass growth will have a negligible effect on the high-mass galaxies.

3 REDSHIFT-DEPENDENT BIASES

To ensure that any conclusions based on our sample are reliable, we must first explore any potential redshift-dependent biases that may affect our results. Our final result is based on the trends of bar fraction in the sample of disc galaxies, so we must determine whether we can detect bars in all galaxies across the whole redshift range, particularly for galaxies with smaller radii (addressing the numerator in our bar fraction measurement). We must also explore whether surface brightness dimming affects a GZH volunteer's ability to classify a galaxy as disc-like, especially towards higher redshifts (i.e. the denominator of the bar fraction measurement).
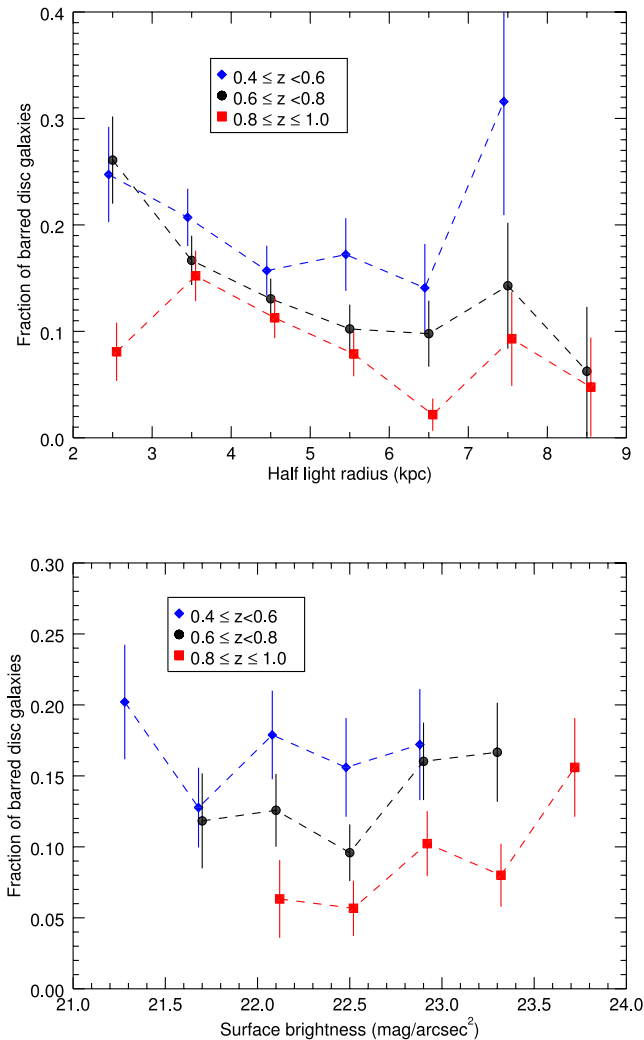
As our work and that of S08 both use the same imaging data, we point the reader to the extensive discussion by S08 of the impact of selection effects (their appendices A1-A4). Much of the discussion in these appendices is directly applicable to this work, with the exception of A2. This section explores the possible inclusion of objects with peculiar morphology affecting the bar fraction when using ellipticity and position angle information to determine morphological classifications, which is not relevant for our sample of visually selected disc galaxies. We note that the effects of band shifting across this redshift range have already been discussed in Section 2.1.

3.1 Spatial resolution

As the ACS is capable of resolving all structures larger than 2 kpc across our specified redshift range (see Section 2.1), we are confident that all large-scale bars should be detectable in our GZH

sample. In the local Universe, bars smaller than 2 kpc in massive disc galaxies are classified as nuclear bars (Erwin 2004), which are not the bars we are concerned with in this study. Additionally, in their appendix A4, S08 find there is little change in the median disc scale length for their sample of disc galaxies up to $z \sim 1$ (also see Ravindranath et al. 2004; Barden et al. 2005; Sargent et al. 2007). They conclude the lack of change in the size of disc galaxies over this redshift range should therefore mean that the sizes of bars will also remain unchanged.

Following S08 (A4), we explore the effects of resolution further by examining how the bar fraction of GZH sample depends on disc galaxy size (Fig. 6, top) in three redshift bins ($0.4 \leq z < 0.6$; $0.6 \leq z < 0.8$; $0.8 \leq z \leq 1.0$). If bars were missing in smaller galaxies due to problems with resolution, we should observe this effect in a trend of decreasing f_{bar} for the smallest galaxies, and specifically this should be largest in the highest redshift bin. In fact, the data show that for the low- and intermediate-redshift bins we see a declining bar fraction towards larger disc galaxies, while the

high-redshift bin shows little change in the bar fraction across all galaxy sizes.

Finally, we also explored the redshift evolution of the bar fraction in three angular size bins, finding that our overall result (see Section 4.1) is observed in all three bins.

We conclude that the effects of resolution do not cause large-scale bars to be lost in any size of galaxy. Therefore, an inability to detect and classify bars does not bias our final results.

3.2 Surface brightness

Surface brightness dimming has the potential to have a significant impact as it evolves strongly with redshift. It may cause disc galaxies to be missing from the sample entirely, or to be misclassified either as 'smooth' galaxies (in the language of GZH), or potentially in the case of barred galaxies as inclined discs (if the outer disc fades leaving only the bar visible).

S08 (see their A3) investigate the ability of COSMOS imaging to trace the outer discs of galaxies as a function of redshift in an attempt to quantify this effect. Their fig. 10 demonstrates that COSMOS imaging is sufficiently able to detect the outer parts of typical disc galaxies out to $z = 1$.

In addition, they suggest an empirical test to see how the bar fraction depends on surface brightness. This is done by comparing the bar fraction as a function of the observed surface brightness of the discs in three redshift bins (the same bins used in Section 3.1). Any impact of surface brightness dimming on the bar fraction would be revealed by a correlation of bar fraction with surface brightness, and specifically should be largest in the highest redshift bin. We observe no correlation of the bar fraction with surface brightnesses for each of the redshift bins when conducting this test using our GZH disc sample (Fig. 6, bottom). This observed constant bar fraction with surface brightness demonstrates that bars/discs are equally detectable in the dimmest galaxies to the brightest disc galaxies.

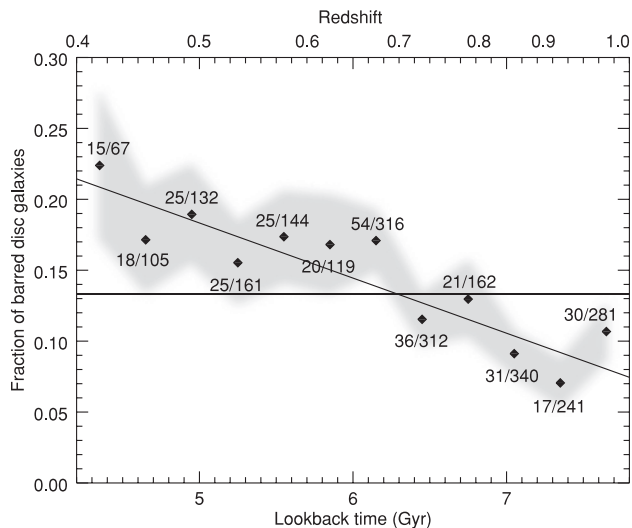We conclude that surface brightness dimming does not bias our final results.

4 RESULTS

4.1 Redshift evolution of the bar fraction

We explore the trend of the bar fraction, f_{bar}, across ~ 3.6 Gyr of cosmic history, from a lookback time of $t_{lb} = 4.2$ Gyr (at $z = 0.4$) to $t_{lb} = 7.8$ Gyr ($z = 1.0$). The redshift evolution of the bar fraction is observed in Fig. 7, where the fraction of barred galaxies decreases from $f_{bar} = 22 \pm 5$ per cent at $t_{lb} = 4.2$ Gyr ($z = 0.4$) to $f_{bar} = 11 \pm 2$ per cent at $t_{lb} = 7.8$ Gyr ($z = 1.0$). We show that a linear relationship (bold line) offers a good fit to our observations, with this relationship given in Table 1.

Our GZH disc sample is split into equal time bins, with the bar fraction calculated for each 0.3 Gyr interval, which approximately corresponds to redshift bins of ~ 0.05. Although this is fine binning for the use of photometric redshifts, it is appropriate, as the photometric redshifts of our galaxies are accurate to $\sigma_{\Delta_z} \lesssim 0.02$ up to $z = 1.25$ (Ilbert et al. 2009). Each point is labelled with the number of barred disc galaxies (N_{bar}) over the total number of disc galaxies (N_{disc}) observed within the given bin. We show 1σ errors for each point (grey), with the errors calculated as follows:

$$\sigma_f = \sqrt{\frac{f_{bar}(1 - f_{bar})}{N_{disc}}}.$$

Figure 6. Potential biases in the GZH sample. The GZH sample is split into three redshift bins; $0.4 \leq z < 0.6$ (blue), $0.6 \leq z < 0.8$ (black) and $0.8 \leq z \leq 1.0$ (red). Top – the bar fraction as a function of half light radius (kpc) for each of these bins with a minimum of 15 disc galaxies required for a data point to be shown. Bottom – the bar fraction as a function of surface brightness.

Figure 7. Redshift evolution of the fraction of barred disc galaxies. Each point represents the observed bar fraction in a 0.3 Gyr bin, with the number of barred disc galaxies and total number of disc galaxies indicated. The grey tramlines represent a 1σ error for the points. We show the mean bar fraction for the whole sample ($f_{\rm bar} = 13.3 \pm 0.7$ per cent) as the horizontal dot–dashed line, as well as a linear relationship between the bar fraction and the lookback time, which is shown by the solid line. Our shaded errors do not account for any systematic errors that may be present, especially in the higher redshift bins.

Table 1. Linear equations in the form $f_{\rm bar} = f_{\rm bar,0} + (\gamma\, t_{\rm lb}({\rm Gyr}))$, which relates the bar fraction evolution to lookback time for the full GZH disc sample and the three stellar mass subsamples. Linear relationships for the three mass subsamples are shown in Fig. 8 with only the GZH data points considered. We also show the relationships which include the GZ2 points in the table below.

Sample (GZH data only)	$f_{\rm bar,0}$	γ
GZH (Fig. 7)	0.38 ± 0.05	-0.039 ± 0.008
Low mass	0.27 ± 0.08	-0.024 ± 0.013
Intermediate mass	0.33 ± 0.08	-0.036 ± 0.012
High mass	0.50 ± 0.11	-0.052 ± 0.016
Sample (GZH + GZ2 data)	$f_{\rm bar,0}$	γ
Low mass	0.16 ± 0.01	-0.006 ± 0.002
Intermediate mass	0.26 ± 0.01	-0.024 ± 0.002
High mass	0.40 ± 0.01	-0.035 ± 0.002

Our result is consistent with that of S08, whose observed strong bar fraction decreased from $f_{\rm bar} = 35 \pm 5$ per cent to $f_{\rm bar} = 17 \pm 2$ per cent across the redshift range they explored ($0.2 < z < 0.84$). See Section 5.1.1 for more details on the comparison between our results and those of S08. We are also consistent with the observations of Jogee et al. (2004) and Cameron et al. (2010).

4.2 Galaxy mass-dependent redshift evolution of the bar fraction

We split the GZH disc sample into three separate mass bins (as described in Section 2.4), enabling us to explore the mass dependence of the evolving bar fraction with time. These observations are shown in Fig. 8, with the low-redshift GZ2 data also shown in equivalent
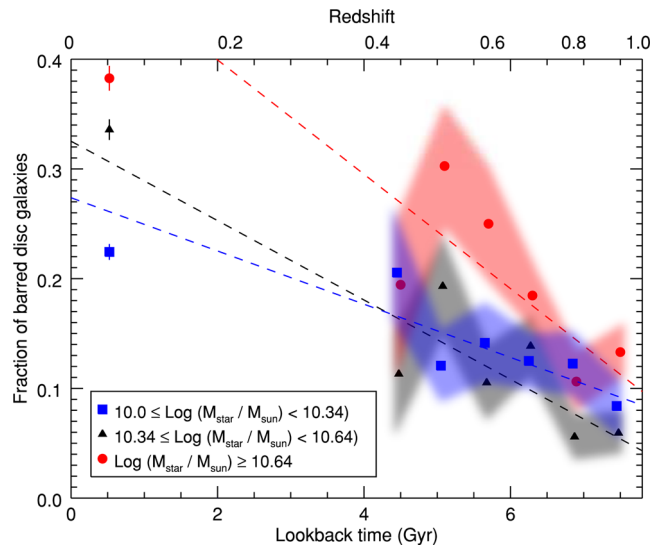
Figure 8. Redshift evolution of the bar fraction split into three mass bins of $\log(M_\star/M_\odot) = 10.0$–$10.34$ (blue squares), 10.34–10.64 (black triangles) and ≥ 10.64 (red circles). Low-redshift points from GZ2 with the same mass limits are also included. Also shown are linear relationships for each mass bin (dashed lines). The relationships shown do not include the GZ2 points. These equations can be found in Table 1, along with linear equations that do include the GZ2 data points. Our shaded errors do not account for any systematic errors that may be present, especially in the higher redshift bins.

mass bins. The GZH disc sample is split into 0.6 Gyr bins (which span $t_{\rm lb} = 4.2$–7.8 Gyr), with the GZ2 data representing a bin of 0.57 Gyr ($t_{\rm lb} = 0.23$–0.80 Gyr, or $z = 0.01$–0.06).

We find that the increase in bar fraction over cosmic time is driven by the most massive galaxies. Specifically we observe the following.

1. *Low-mass subsample:* We observe a slow evolution of the bar fraction within the 1σ errors shown in Fig. 8, with the bar fraction decreasing by a factor of 2.2 over 4.2 Gyr, from $f_{\rm bar} = 21 \pm 5$ per cent at $t_{\rm lb} = 4.2$ Gyr to $f_{\rm bar} = 9 \pm 3$ per cent at $t_{\rm lb} = 7.8$ Gyr. Extending this to the local Universe GZ2 sample, we see that the bar fraction ($f_{\rm bar} = 22 \pm 1$ per cent) has only increased slightly since $z = 0.4$. The shallow decrease in bar fraction towards higher redshifts for the GZH low-mass discs is illustrated by a linear fit shown in Fig. 8 (blue dashed line), with the parameters of this fit given in Table 1. We also show in Table 1 the linear equation when the GZ2 data point is included, which gives a shallower evolution of the bar fraction for these galaxies over the 8 Gyr explored.

2. *Intermediate-mass subsample:* the bar fraction almost halves from $f_{\rm bar} = 11 \pm 4$ per cent at $t_{\rm lb} = 4.2$ Gyr to $f_{\rm bar} = 7 \pm 2$ per cent at $t_{\rm lb} = 7.8$ Gyr. Extending this to the GZ2 sample, we find that the bar fraction is higher ($f_{\rm bar} = 34 \pm 1$ per cent) than at $z = 0.4$ in the GZH sample. Overall, the bar fraction for intermediate galaxies decreases by around a factor of 5 across the full 8 Gyr. We fit a linear trend to this subsample (dashed black line in Fig. 8), with the equation shown in Table 1.

3. *High-mass subsample:* we observe a decrease in the bar fraction with redshift, from $f_{\rm bar} = 30 \pm 5$ per cent at $z = 0.5$ to $f_{\rm bar} = 12 \pm 2$ per cent at $z = 0.8 - 1$. Extending this to the GZ2 sample, the bar fraction has increased to $f_{\rm bar} = 38 \pm 1$ per cent at $z = 0$. Over the full 8 Gyr, the bar fraction has increased by a factor of 3. A linear fit for our high-mass sample (red dashed line on Fig. 8) is given in Table 1.

5 DISCUSSION

Our visually classified GZH disc sample shows a decreasing bar fraction with increasing redshift. More specifically, the bar fraction decreases from $f_{bar} = 22 \pm 5$ per cent down to $f_{bar} = 11 \pm 2$ per cent across the 3.6 Gyr ($0.4 \leq z \leq 1.0$) explored (Fig. 7). When splitting the GZH disc sample into three subsamples by galaxy mass (Fig. 8), we find that the low-mass and intermediate-mass galaxies have slowly increasing bar fractions towards lower redshifts, while the high-mass galaxies have a much steeper increase in bar fraction towards lower redshifts. When extending our results into the local Universe ($z \sim 0.1$) using the GZ2 disc sample, we find that all trends continue in a similar manner.

In this section we compare our results with other works, both observational and theoretical, which have also explored the redshift evolution of the bar fraction. We follow this by providing an interpretation of our result.

5.1 Comparison with other work

The literature regarding bar fraction measurements at both high and low redshifts is extensive (see Sellwood 2013 for a recent review). Fig. 9 shows the redshift evolution for our results (black), including the GZ2 bar fraction (as published in M12). In addition to these, we show several other high-redshift studies; Elmegreen et al. (2004) – red; Jogee et al. (2004) – orange; Elmegreen et al. (2005) – pink; S08 – blue; Cameron et al. (2010) – purple. We also include a theoretical prediction of the expected bar fraction

evolution based on the re-simulation of discs embedded in a cosmological simulation (Kraljic et al. 2012; green). Here, we will not attempt to make a comprehensive comparison of our results to all the studies shown in Fig. 9, although it is clear that our observations of a decreasing bar fraction with increasing redshift agree with the picture built by the combination of these results. Instead, we will compare our results with two particularly relevant studies: S08, whose disc sample is the largest used to explore the redshift evolution of the bar fraction, and the simulated predictions of Kraljic et al. (2012).

5.1.1 Comparison with S08

Following the results of Elmegreen et al. (2004) and Jogee et al. (2004), who concluded that the bar fraction did not evolve with redshift, S08 explored the evolving bar fraction with a carefully selected disc galaxy sample. Their sample was an order of magnitude larger than these previous studies ($N = 2157$), and showed a declining bar fraction with increasing redshift. Our GZH results agree well with S08, although in revisiting their work, we attempt to extend the redshift space explored by allowing for classifications up to $z = 1$.

While the results of S08 and our own are both from the same survey (COSMOS), the processes we use to select our visually classified GZH disc and barred disc samples differ to the selection criteria used by S08. We discuss the selection processes used to determine our GZH disc sample in Section 2.2.
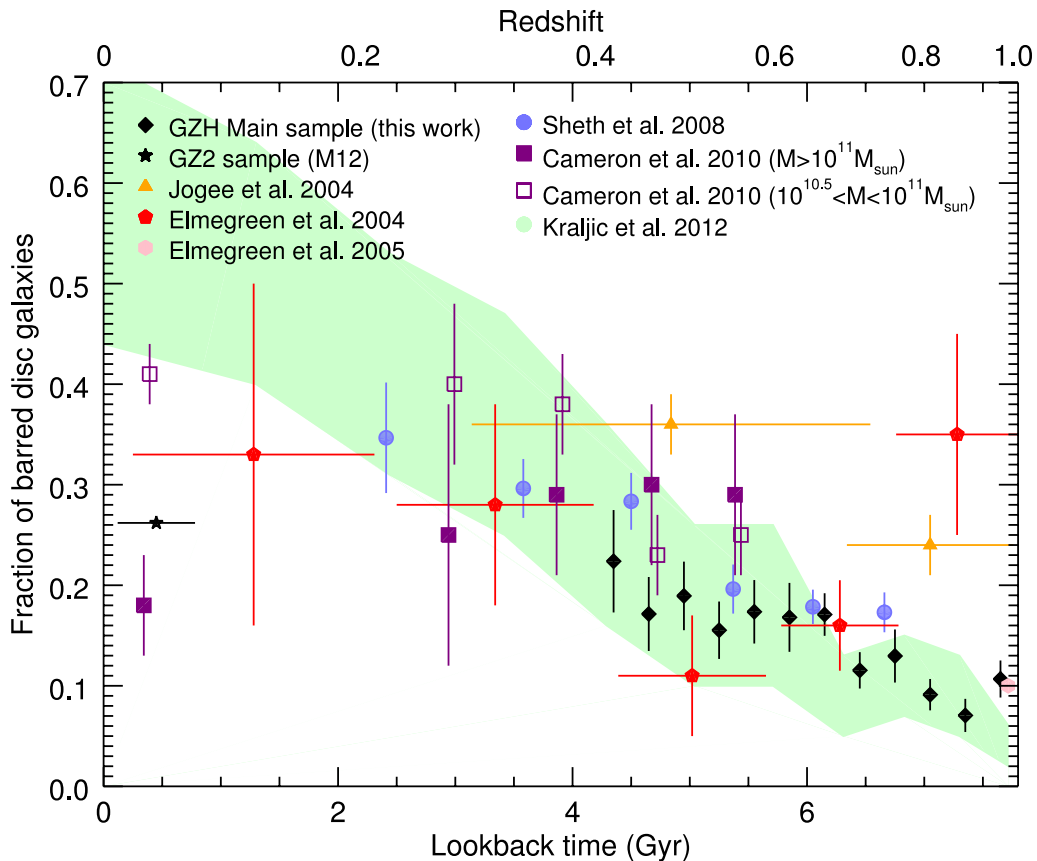
Figure 9. Redshift evolution of the bar fraction from our GZH and GZ2 data (black) compared to the results of several other high-redshift studies; S08 (blue), Elmegreen et al. (2004) (red), Jogee et al. (2004) (orange), Elmegreen et al. (2005) (pink) and Cameron et al. (2010) high- and intermediate-mass samples (purple). We also show a simulated evolution of the bar fraction from Kraljic, Bournaud & Martig (2012) (green).
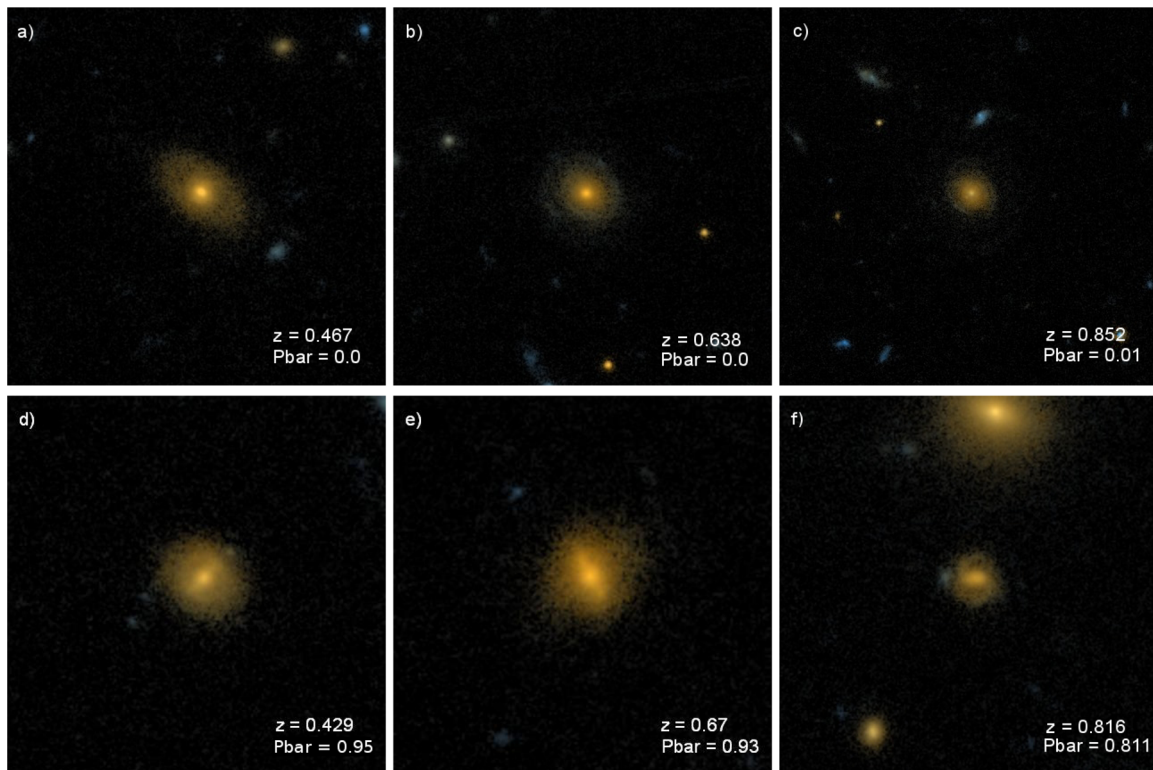
Figure 10. Images showing three unbarred (images a–c) and three barred (images d–f) 'red spiral' galaxies (i.e. visually identified discs with $T_{phot} < 2.0$). The images are organized in ascending redshift for each sample, with the redshift and expected weighted likelihood from GZ classifications that the galaxy hosts a barred structure (p_{bar}) data shown in the bottom right hand corner.

To produce their disc galaxy sample, S08 used spectral energy distribution (SED) classifications based on a match to published templates (see Mobasher et al. 2007 for details). These classifications range from $T_{phot}=1$ to 6, where $T_{phot} = 1$ corresponds to elliptical galaxy, 2=Sbc, 3=Scd, 4=Irr (from Coleman, Wu & Weedman 1980), and types 5 and 6 are starburst models (from Kinney et al. 1996). S08 include only galaxies with $T_{phot} \geq 2$[7] in order to exclude all elliptical and lenticular galaxies from the sample. Applying the same criteria to our own catalogue, we find that 95.9 per cent (2282) of our visually identified disc galaxies have $T_{phot} \geq 2$, with 98 of our GZH disc galaxies categorized with earlier type SEDs. The volume limit and inclination cuts applied by S08 are also different from our selection.

The 98 (4 per cent of the GZH disc sample) disc galaxies we identify with $T_{phot} < 2.0$ are the high-redshift equivalents of 'red spirals' (Masters et al. 2010), which have previously been identified in the COSMOS data (Bundy et al. 2010). In our local Universe up to 20 per cent of disc galaxies are 'red' (Bamford et al. 2009; Skibba et al. 2009), and even among late-type disc galaxies (i.e. Sb and Sc type galaxies) 6 per cent are found near the red sequence (Masters et al. 2010). Of particular relevance to this work is that red spirals in the local Universe are found to have high bar fractions (Masters et al. 2010, 2011). Indeed, among the 98 'red spirals' in our sample, 45 per cent (44) are identified as having a strong bar, compared to 11.5 per cent for late-type galaxies selected by T_{phot}

(i.e. $T_{phot} \geq 2.0$). Example images[8] of some of the red disc galaxies are shown in Fig. 10.

The bar identification used in S08 is also different from our own. S08 identify bars by an ellipse fitting method, and also through visual classifications by a single author, with a cross check of 500 galaxies by a second author. These two methods were cross checked and found to be consistent 85 per cent of the time. We use GZ identifications based on a median of 29 citizen scientists per galaxy.

Despite these variations in selection criteria, both studies observe similar overall trends of bar fraction with redshift (see Fig. 9). We show in Appendix A1 that, by altering the threshold of p_{bar} we use to define our barred GZH sample, we can replicate the absolute bar fraction values observed by S08 (using $p_{bar} = 0.45$), without significantly changing the trend we observe.

Where the studies appear to differ initially, is in the interpretation of the galaxy mass dependence of the redshift evolution of the bar fraction. However, when we only consider the data where the redshift bins and mass ranges are directly comparable [$0.4 < z < 0.84$ and $\log(M_\star/M_\odot) \gtrsim 10.3$], we find that the qualitative trends are in agreement.

5.1.2 Comparison with predictions of Kraljic et al. (2012)

There has been substantial progress in the theoretical modelling of bar formation in disc galaxies (e.g. Combes & Sanders 1981; Berentzen et al. 1998; Athanassoula 2003; Debattista et al. 2006;

---

[7] This differs from the published selection ($T_{phot} > 2$) due to a typographical error in publication (K. Sheth, private communication.)

[8] Images of all 98 red spirals are shown at http://data.galaxyzoo.org/GZH/samples/tphot_disks.html

Martinez-Valpuesta, Shlosman & Heller 2006; Villa-Vargas, Shlosman & Heller 2009; Saha & Naab 2013). The realization that the transfer of angular momentum between dark matter haloes and the gaseous component in disc galaxies was vital to the growth of bars over time (e.g. Athanassoula 2003), along with improvements in computational power, has led to a significant increase in the sophistication of bar modelling.

Of particular interest to this work is Kraljic et al. (2012) who published a prediction for the redshift evolution of the bar fraction for a sample of 33 simulated disc galaxies which they followed over cosmic history. Initially part of a full cosmological dark matter simulation (see Martig et al. 2012 for details), the 33 galaxies were selected to have $z = 0$ masses of $\log(M_\star/M_\odot) = 10$–11.3. Kraljic et al. re-simulated these galaxies using a 'zoom-in' technique, with a 'sticky-particle' scheme used to model interstellar gas dynamics. The re-simulations began at $z = 5$, and the evolution of the galaxies were traced from $z = 2$ to $z = 0$. For more information, including the method of bar identification and other analysis, see Kraljic et al. (2012) and Martig et al. (2012).

The work of Kraljic et al. (2012) provides an interesting theoretical comparison to our observed results for two main reasons. First, the present day (and $z = 1$; see Martig et al. 2012) mass range explored is similar to the stellar mass ranges in our observed sample, and secondly, these simulations focus on disc-like galaxies, and a range of bar strengths are available to compare against.

We show in Fig. 9 that, over the range of lookback times explored by our GZH data, the predicted evolution of the bar fraction in Kraljic et al. (2012) (green tramlines which represent Poissonian errors) agrees with our observations (and those of S08).

At lower redshifts ($z < 0.2$), we do not agree with Kraljic et al. (2012). The simulations predict a strong bar fraction of 58 per cent: considerably higher than that observed in GZ2 ($f_{bar} = 26$ per cent). Their strong bar fraction prediction does agree with other published values of the bar fraction in the local Universe (e.g. Barazza, Jogee & Marinova 2003; Aguerri et al. 2009); however, these observations include both strong and weak bars.
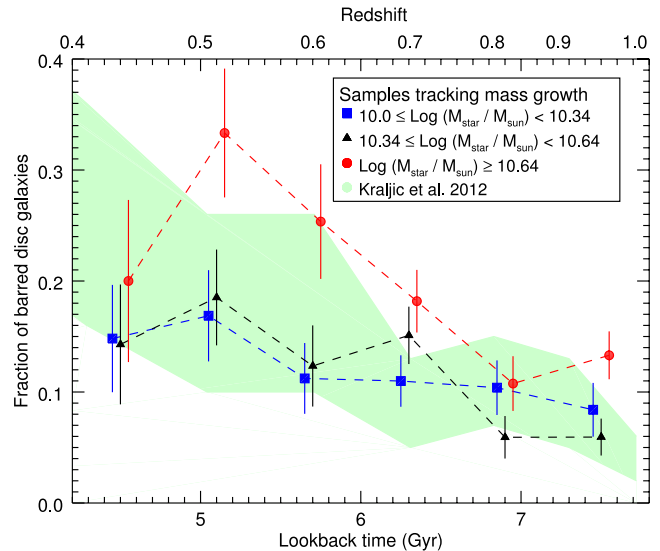
We note that in Kraljic et al. (2012), the strong bar fraction is observed in the same 33 discs as they are tracked through their evolution (see fig. 6 from Kraljic et al. 2012), while our GZH observations show only how the bar fraction in a population of galaxies of a given mass range changes with redshift. Here, we attempt to make a fairer comparison by exploring the bar fraction for three mass evolving disc galaxy subsamples.

We assume a typical SFR of $1.5\,M_\odot\,yr^{-1}$. This value is approximately the expected SFR of these disc galaxies over the 3.6 Gyr explored (1–$2\,M_\odot\,yr^{-1}$; Damen et al. 2009; van Dokkum et al. 2010; Karim et al. 2011), with significantly lower SFRs only found in massive elliptical galaxies and higher for rare starburst galaxies.

Table 2 shows the initial stellar mass ranges for our three subsamples (as described in Section 2.4), and their corresponding mass ranges after 3.6 Gyr have elapsed. The result of including the effects of star formation, and therefore mass growth, means that galax-

Figure 11. Redshift evolution of the bar fraction for three evolving stellar mass bins: low mass (blue squares), intermediate mass (black triangles) and high mass (red circles). The initial $z = 1.0$ mass ranges are those described in Section 2.4, with these and the final ($z = 0.4$) mass ranges given in Table 2.

ies which are of low or intermediate mass at $z = 1.0$ may have accumulated sufficient mass to be moved into a higher mass bin by $z = 0.4$. The most massive galaxies at $z = 1.0$ are less affected by mass growth, as the accumulation of $1.5\,M_\odot\,yr^{-1}$ is negligible for them.

The result of including star formation is shown in Fig. 11. With the incorporation of stellar mass growth, we find that our observations are still in agreement with those simulated by Kraljic et al. (2012) at higher redshifts ($z > 0.4$).

5.2 Implications – the role of stellar mass in bar formation and evolution

The observations presented in Fig. 8 show that the evolution of bar fraction with time is dependent on stellar mass, with the bar fraction of the most massive disc galaxies ($f_{bar} = 38.3$ per cent) being almost double that of our low-mass disc galaxies ($f_{bar} = 22.4$ per cent) by $z = 0$. Additionally, the lowest mass disc galaxies we track [$\log(M_\star/M_\odot) = 10.0$–10.34] show the shallowest evolution of the bar fraction, increasing by 2 per cent per Gyr over 8 Gyr, compared to 6 per cent per Gyr for the most massive.

When interpreting these differing trends we observe for each mass subsample, it is important to remember that the bar fraction is not only dependent on the number of bars present in each time bin (N_{bar}), but also on the number of disc galaxies (N_{disc}). If we first look at our high-mass sample, it is a reasonable assumption that most massive disc galaxies are in place by $z \sim 1$, and so N_{disc} will remain approximately constant across the 8 Gyr explored. Therefore, the steep bar fraction evolution we see in our high-mass sample is being driven by an increasing N_{bar} towards lower redshifts.

Bars are predicted to form quickest in massive, dynamically cool stellar discs (Athanassoula 2005; Athanassoula et al. 2009; Cheung et al. 2013), and are long lived structures (e.g. Debattista et al. 2006; Athanassoula, Machado & Rodionov 2013, but see Combes 2008 or Bournaud & Combes 2002 for an opposing view). The results we present support this theory, as it is the most massive disc galaxies that are more likely to host bars at earlier times.

Table 2. Initial ($z = 1.0$) and final ($z = 0.4$) mass ranges for three mass evolving GZH subsamples when a SFR of $1.5\,M_\odot\,yr^{-1}$ is applied.

Mass sample	$z = 1.0$ mass range	$z = 0.4$ mass range
Low mass	10.0–10.34	10.16–10.42
Intermediate mass	10.34–10.64	10.42–10.68
High mass	≥10.64	≥10.68

S08, Sheth et al. (2012) and Cameron et al. (2010) all observed the bar fraction to be highest in the most massive galaxies at high redshifts, with Kraljic et al. (2012) also showing that their more massive simulated galaxies formed their bars earliest. At low redshifts, such as the range explored by the GZ2 sample, it is observed that strong bars are more likely to be found in more massive galaxies (see Nair & Abraham 2010; Skibba et al. 2012). This can all be explained by massive galaxies becoming dynamically cool, disc dominated quicker (i.e. N_{disc} is constant at $z \lesssim 1$ for massive disc galaxies) and having lower gas fractions than their lower mass counterparts.

The increasing bar fraction we observe in the most massive disc galaxies over the 3.6 Gyr coincides with a proposed first epoch of substantial bar formation at z=0.8–1 (Kraljic et al. 2012), who suggest that secular processes begin to dominate the evolution of massive disc galaxies at $z < 1.0$. Our observations are consistent with this picture, as it is the increasing N_{bar} that drives the rapid evolution of the bar fraction for our high-mass disc galaxies.

Alternatively, we observe a population of lower mass disc galaxies whose bar fraction increases at a much slower rate compared to that seen for the more massive disc galaxies. For these discs, we will assume that N_{bar} increases at a similar rate to that for higher mass galaxies. However, for our low-mass sample we expect that N_{disc} is also increasing towards lower redshifts, and so the overall increase in the bar fraction is much shallower than observed in our high-mass discs.

Nair & Abraham (2010) observed a bimodality in the fraction of bars in $z = 0$ disc galaxies with a minimum at the typical mass transition of the colour–magnitude diagram [$\log(M_{\star}/M_{\odot}) = 10.2$]. They suggest the bimodality could be revealing fundamental differences in bar formation mechanisms in these two regimes and postulate that bars may be more easily triggered, and will form more quickly in lower mass disc galaxies. They also state that bars would be easier to destroy in these lower mass galaxies. In this scenario, the relatively low increase in bar fraction we see in our lowest mass subsample [$\log(M_{\star}/M_{\odot}) = 10.0$–10.34] over 8 Gyr can be explained by the combination of both the balance between the time-scales of these two processes across cosmic time and the continually increasing number of unbarred disc galaxies (N_{disc}) entering our sample towards lower redshifts. In higher mass galaxies, bars are predicted to be more stable, so once formed, they will persist over long periods. The monotonic increase in bar fraction we observe for these galaxies is consistent with this explanation.

More recently, works with smaller samples of $z = 0$ galaxies (Méndez-Abreu, Sánchez-Janssen & Aguerri 2010; Méndez-Abreu et al. 2012; Sheth et al., in preparation) do not observe the low-mass peak in the bar fraction. In this scenario the low increase of the bar fraction in our lowest mass galaxies can be interpreted as these disc galaxies not yet having bars.

The differing rates of increase we observe in the evolution of the bar fraction for different mass galaxies suggest more than one process is at play in determining the observed bar fraction; affecting both rates of bar formation in discs (N_{bar}), as well as the rate of galaxies becoming disc dominated (N_{disc}). We review possible mass-dependent processes that could affect these time-scales:

Gas content: simulations suggest that increasing the gas fraction in disc galaxies will inhibit bar formation (e.g. Friedli & Benz 1993; Berentzen et al. 2007; Heller, Shlosman & Athanassoula 2007; Villa-Vargas, Shlosman & Heller 2010; Kraljic, Bournaud & Martig 2012; Athanassoula et al. 2013), with observations offering support to these theories (Masters et al. 2012). Correlations exist between the total gas content of disc galaxies and their stellar mass (e.g. Kauffmann et al. 2003a; Catinella et al. 2010, 2012), such that more massive disc galaxies tend to be less gas rich. The gas content of disc galaxies is also known to decrease over cosmic time (e.g. Tacconi et al. 2013), which can naturally explain the increasing bar fractions of the massive and intermediate - galaxies as they gradually lose their gas. In this scenario, the lower mass galaxies that continuously enter our low-mass sample towards lower redshifts start out unbarred, and may remain unable to form strong bars even to $z \sim 0$. However, the situation may be different for weaker bars, which are still able to form and grow, albeit at a slower rate, in gas-rich galaxies (Athanassoula et al. 2013), and so they may be more abundant in these gas-rich galaxies (e.g. Nair & Abraham 2010).

Tidal heating: the impact that tidal heating, or harassment (i.e. minor mergers adding random motion to the stellar disc), has on a galaxy will depend sensitively on its mass. S08, Sheth et al. (2012) and Giordano et al. (2011) have all argued that this effect may drive the different evolutions of the bar fraction observed in disc galaxies with differing masses (with redshift and environment, respectively). Interactions which would act to trigger bar formation in more massive galaxies (e.g. Moore et al. 1996; Skibba et al. 2012) may instead heat the disc of a lower mass galaxy, preventing any bar formation. As cosmic time proceeds, such interactions become less likely as the galaxy number density decreases. This would lead to not only less tidal triggering, but also less inhibition of bar formation from disc heating, and less disruption of bars from more violent encounters. Indeed, the phase of increased bar formation that we observe in the most massive discs in our sample at $z \sim 0.7$ coincides with an observed reduction in major merger rates (see Conselice et al. 2003; Ryan et al. 2008; Lotz et al. 2011). As discussed in Kraljic et al. (2012), prior to $z = 1$ the evolution of galaxies is dominated by violent interactions (such as major and minor mergers). Therefore, as the merger rate begins to decline, the evolution of disc galaxies becomes dominated by secular processes.

How the bar fraction continues to evolve in these different mass regimes at $z > 1$ is of significant interest. Kraljic et al. (2012) make a clear prediction that at $z > 1$, $f_{bar} \sim 0$ as stable discs become rare. We are extending our observations of the bar fraction to higher redshifts, using images from the Cosmic Assembly Near-Infrared Deep Extragalactic Legacy Survey (CANDELS; Grogin et al. 2011; Koekemoer et al. 2011). These images are currently being classified by GZ volunteers in the fourth incarnation of GZ.[9]

6 SUMMARY

We present a study of the redshift evolution of the bar fraction from a sample of 2380 disc galaxies. The galaxy images were taken as part of the COSMOS programme, and were visually classified by GZH volunteers. Our GZH disc sample is volume limited [$0.4 \leq z \leq 1.0$; $\log(M_{\star}/M_{\odot}) \geq 10.0$], and does not include highly inclined discs [$\log(a/b) < 0.3$]. The identification of barred structures hosted in these disc galaxies is based on GZH visual classifications. We present evidence that suggests the barred disc galaxies identified in this way host strong bars.

We explore the stellar mass dependence of the redshift evolution of the bar fraction by splitting the GZH sample into three equally populated stellar mass bins: $\log(M_{\star}/M_{\odot}) = 10.0$–10.34; 10.34–10.64 and $\geq$10.64. Our main results and conclusions are as follows.

[9] www.galaxyzoo.org

(i) We observe a decrease in the bar fraction towards higher redshifts, with the overall reduction being a factor of 2 across 3.6 Gyr of cosmic time, from $f_{bar} = 22 \pm 5$ per cent at $t_{lb} = 4.2$ Gyr ($z = 0.4$) to $f_{bar} = 11 \pm 2$ per cent at $t_{lb} = 7.8$ Gyr ($z = 1.0$).

(ii) We find that splitting the GZH sample by stellar mass reveals differing redshift evolution of the bar fraction. Lower mass disc galaxies are observed to have a steady but slowly decreasing bar fraction towards $z = 1$, with the intermediate-mass galaxies having a similar, but slightly steeper decrease.

(iii) The steepest decrease in bar fraction evolution is seen in the most massive disc galaxies, with this trend observed across the whole 8 Gyr explored. We suggest that the redshift evolution of the bar fraction we find is predominantly driven by the evolution observed in these high-mass disc galaxies.

(iv) An extrapolation of the trends we see to higher redshifts suggests that we may be observing an era of transition in disc galaxy evolution, where secular processes have recently begun to affect the evolution of some of the more massive disc galaxies. At this epoch, we suggest that the first galaxies have become dynamically cool and disc dominated and are able to form and sustain barred structures. This time coincides with a decreasing rate of major mergers in these same massive galaxies (Conselice et al. 2003; Ryan et al. 2008; Lotz et al. 2011).

(v) The slow evolution of the bar fraction observed for lower mass disc galaxies suggests that different processes may dominate bar formation and disruption in these galaxies. The suggestion that lower mass disc galaxies may host different types of bars with separate formation processes has previously been made by Nair & Abraham (2010), based on the bimodal trend of bar fraction with galaxy mass they observed in the local Universe.

(vi) We combine GZH visual classifications with T_{phot} values (see Mobasher et al. 2007) to identify a subsample of 98 quiescent disc galaxies. The bar fraction of these discs, $f_{bar} = 44.9 \pm 5$ per cent, is a factor of 3.8 greater than the bar fraction observed across the whole GZH sample ($f_{bar} = 13.3$ per cent), as well as being a factor of 3.9 times greater than the bar fraction observed in late-type (i.e. $T_{phot} \geq 2.0$) galaxies ($f_{bar} = 11.5$ per cent).

This paper provides the first results from the third incarnation of the Galaxy Zoo project, Galaxy Zoo: Hubble. The observations we have discussed identify an important point in a disc galaxy's lifetime, where the regime of dramatic and dynamically quick evolutionary processes curtail and an epoch of a calmer (secular) evolution begins. We demonstrate that this point in a galaxy's evolution can be identified simply by exploring its morphological features, specifically whether the galaxy in question hosts a barred structure.

REFERENCES

Abraham R. G., 1999, in Barnes J. E., Sanders D. B., eds, Galaxy Interactions at Low and High Redshift. IAU Symp. Vol. 186, A Review of High-Redshift Merger Observations. p. 11

Abraham R., Merrifield M., Ellis R., Tanvir N., Brinchmann J., 1999, MNRAS, 308, 569

Aguerri J. A. L., Méndez-Abreu J., Corsini E. M., 2009, A&A, 495, 491

Alonso M. S., Coldwell G., Lambas D. G., 2013, A&A, 549, A141

Athanassoula E., 2003, MNRAS, 341, 1179

Athanassoula E., 2005, Celest. Mech. Dyn. Astron, 91, 9

Athanassoula E., 2012, preprint (arXiv:1211.6752)

Athanassoula E., Gadotti D. A., Carrasco L., Bosma A., de Souza R. E., Recillas E., 2009, preprint (arXiv:0910.0768)

Athanassoula E., Machado R. E. G., Rodionov S. A., 2013, MNRAS, 429, 1949

Baillard A. et al., 2011, A&A, 532, A74

Baldry I. K., Glazebrook K., Brinkmann J., Ivezic Z., Lupton R. H., Nichol R. C., Szalay A. S., 2004, ApJ, 600, 681

Bamford S. P. et al., 2009, MNRAS, 393, 1324

Barazza F. D., Jogee S., Marinova I., 2003, ApJ, 675, 1194

Barazza F. D., Jogee S., Marinova I., 2008, ApJ, 675, 1194

Barden M. et al., 2005, ApJ, 635, 959

Barnes J. E., Hernquist L. E., 1991, ApJ, 370, L65

Bennett C. L. et al., 2012, ApJS, 208, 20

Berentzen I., Heller C. H., Shlosman I., Fricke K. J., 1998, MNRAS, 300, 49

Berentzen I., Shlosman I., Martinez-Valpuesta I., Heller C. H., 2007, ApJ, 666, 189

Bournaud F., Combes F., 2002, A&A, 392, 83

Bundy K. et al., 2006, ApJ, 651, 120

Bundy K. et al., 2010, ApJ, 719, 1969

Cameron E. et al., 2010, MNRAS, 409, 346

Capak P. et al., 2007, ApJS, 172, 99

Catinella B. et al., 2010, MNRAS, 403, 683

Catinella B. et al., 2012, A&A, 544, A65

Cheung E. et al., 2013, ApJ, 779, 162

Cisternas M. et al., 2013, ApJ, 776, 50

Coelho P., Gadotti D. A., 2011, ApJ, 743, L13

Coleman G. D., Wu C.-C., Weedman D. W., 1980, ApJS, 43, 393

Combes F., 2008, in Bureau M., Athanassoula E., Barbuy B., eds, Proc. IAU Symp. Vol. 245, Gaseous Flows in Galaxies. p. 151

Combes F., 2009, in Jogee S., Marinova I., Hao L., Blanc G. A., eds, ASP Conf. Ser. Vol. 419. Galaxy Evolution: Emerging Insights and Future Challenges. Secular Evolution and the Assembly of Bulges. Astron. Soc. Pac., San Francisco, p. 31

Combes F., Sanders R. H., 1981, A&A, 96, 164

Conselice C. J., Bershady M. A., Dickinson M., Papovich C., 2003, AJ, 126, 1183

Conselice C. J., Rajgor S., Myers R., 2008, MNRAS, 386, 909

Cox T. J., Jonsson P., Somerville R. S., Primack J. R., Dekel A., 2008, MNRAS, 384, 386

Damen M., Labbé I., Franx M., van Dokkum P. G., Taylor E. N., Gawiser E. J., 2009, ApJ, 690, 937

de Vaucouleurs G., de Vaucouleurs A., Corwin J. H. G., Buta R. J., Paturel G., Fouqué P., 1991, Third Reference Catalogue of Bright Galaxies. Springer-Verlag, Berlin

Debattista V. P., Mayer L., Carollo C. M., Moore B., Wadsley J., Quinn T., 2006, ApJ, 645, 209

Ellison S. L., Nair P., Patton D. R., Scudder J. M., Mendel J. T., Simard L., 2011, MNRAS, 416, 2182

Elmegreen B. G., Elmegreen D. M., 1985, ApJ, 288, 438

Elmegreen B. G., Elmegreen D. M., Hirst A. C., 2004, ApJ, 612, 191

Elmegreen D. M., Elmegreen B. G., Rubin D. S., Schaffer M. A., 2005, ApJ, 631, 85

Elmegreen D. M., Elmegreen B. G., Marcus M. T., Shahinyan K., Yau A., Petersen M., 2009, ApJ, 701, 306, 329

Erwin P., 2004, A&A, 415, 941

Friedli D., Benz W., 1993, A&A, 268, 65

Gilmore G., Wyse R. F. G., Norris J. E., 2002, ApJ, 574, L39

Giordano L., Tran K.-V. H., Moore B., Saintonge A., 2010, preprint (arXiv:1111.1532)

Griffith R. L. et al., 2012, ApJS, 200, 9

Grogin N. A. et al., 2011, ApJS, 197, 35

Hawarden T. G., Mountain C. M., Leggett S. K., Puxley P. J., 1986, MNRAS, 221, 41 p

Heller C. H., Shlosman I., Athanassoula E., 2007, ApJ, 657, L65

Ho L. C., Filippenko A. V., Sargent W. L. W., 1997, ApJ, 487, 591

Hopkins P. F., Cox T. J., Younger J. D., Hernquist L., 2009, ApJ, 691, 1168

Hoyle B. et al., 2011, MNRAS, 415, 3627

Ilbert O. et al., 2009, ApJ, 690, 1236

Ilbert O. et al., 2010, ApJ, 709, 644

Ilbert O. et al., 2013, A&A, 556A, 551

Jogee S. et al., 2004, ApJ, 615, L105

Karim A. et al., 2011, ApJ, 730, 61

Kartaltepe J. S. et al., 2010, ApJ, 721, 98

Kassin S. A. et al., 2007, ApJ, 660, L35

Kauffmann G. et al., 2003a, MNRAS, 341, 33

Kauffmann G. et al., 2003b, MNRAS, 341, 54

Kinney A. L., Calzetti D., Bohlin R. C., McQuade K., Storchi-Bergmann T., Schmitt H. R., 1996, ApJ, 467, 38

Knapen J. H., Shlosman I., Peletier R. F., 2000, ApJ, 529, 93

Koekemoer A. M. et al., 2011, ApJS, 197, 36

Kormendy J., Kennicutt R. J., 2004, ARA&A, 42, 603

Kraljic K., Bournaud F., Martig M., 2012, ApJ, 575, 60

Land K. et al., 2008, MNRAS, 388, 1686

Lilly S. J. et al., 2007, ApJS, 172, 70

Lilly S. J. et al., 2009, VizieR Online Data Catalog, 217, 20070

Lin L. et al., 2008, ApJ, 681, 232

Lintott C. J. et al., 2008, MNRAS, 389, 1179

Lintott C. et al., 2011, MNRAS, 410, 166

Lotz J. M., Jonsson P., Cox T., Croton D., Primack J. R., Somerville R. S., Stewart, K., 2011, ApJ, 742, 103

Martig M., Bournaud F., Croton D. J., Dekel A., Teyssier R., 2012, ApJ, 756, 26

Martinet L., Friedli D., 1997

Martinez-Valpuesta I., Shlosman I., Heller C., 2006, ApJ, 637, 214

Masters K. L. et al., 2010, MNRAS, 405, 783, 799

Masters K. L. et al., 2011, MNRAS, 411, 2026

Masters K. L. et al., 2012, MNRAS, 424, 2180 (M12)

Méndez-Abreu J., Sánchez-Janssen R., Aguerri J. A. L., 2010, ApJ, 711, L61

Méndez-Abreu J., Sánchez-Janssen R., Aguerri J. A. L., Corsini E. M., Zarattini S., 2012, ApJ, 761, L6

Menéndez-Delmestre K., Sheth K., Schinnerer E., Jarrett T. H., Scoville N. Z., 2007, ApJ, 657, 790

Mobasher B. et al., 2007, ApJS, 172, 117

Moore B., Katz N., Lake G., Dressler A., Oemler A., 1996, Nature, 379, 613

Mulchaey J. S., Regan M. W., 1997, ApJ, 482, L135

Nair P. B., Abraham R. G., 2010, ApJ, 714, L260

Oh S., Oh K., Yi S. K., 2012, ApJS, 198, 4

Pfenniger D., Norman C., 1990, ApJ, 363, 391

Ravindranath S. et al., 2004, ApJ, 604, L9

Regan M. W., Mulchaey J. S., 1999, AJ, 117, 2676

Ryan J. R. E., Cohen S. H., Windhorst R. A., Silk J., 2008, ApJ, 678, 751

Saha K., Naab T., 2013, MNRAS, 434, 1287

Saintonge A. et al., 2012, ApJ, 758, 73

Sakamoto K., Okumura S. K., Ishizuki S., Scoville N. Z., 1999, ApJ, 525, 691

Sargent M. T. et al., 2006, ApJS, 172, 434

Schawinski K. et al., 2013, submitted

Scoville N. et al., 2007a, ApJS, 172, 38

Scoville N. et al., 2007b, ApJS, 172, 1

Sellwood J. A., 2013, Dynamics of Disks and Warps. p. 923

Sérsic J. L., Pastoriza M., 1965, PASP, 77, 287

Sheth K., Regan M. W., Scoville N. Z., Strubbe L. E., 2003, ApJ, 592, L13

Sheth K., Menendez-Delmestre K., Scoville N., Jarrett T., Strubbe L., Regan M. W., Schinnerer E., Block D. L., 2004, in Block D. L., Puerari I., Freeman K. C., Groess R., Block E. K., eds, Penetrating Bars Through Masks of Cosmic Dust. Astrophysics and Space Science Library Vol. 319, Using Bars As Signposts of Galaxy Evolution at High and Low Redshifts. p. 405

Sheth K., Vogel S. N., Regan M. W., Thornley M. D., Teuben P. J., 2005, ApJ, 632, 217

Sheth K. et al., 2008, ApJ, 675, 1141 (S08)

Sheth K., Melbourne J., Elmegreen D. M., Elmegreen B. G., Athanassoula E., Abraham R. G., Weiner B. J., 2012, ApJ, 758, 136

Skibba R. A. et al., 2009, MNRAS, 399, 966

Skibba R. A. et al., 2012, MNRAS, 423, 1485

Strauss M. A. et al., 2002, AJ, 124, 1810

Tacconi L. et al., 2013, ApJ, 768, 74

van den Bergh S., 2011, AJ, 141, 188

van Dokkum P. G. et al., 2010, ApJ, 709, 1018

Villa-Vargas J., Shlosman I., Heller C., 2009, ApJ, 707, 218

Villa-Vargas J., Shlosman I., Heller C., 2010, ApJ, 719, 1470

Wang J. et al., 2012, MNRAS, 423, 3486

Weiner B. J. et al., 2006, ApJ, 653, 1027

Willett K. W. et al., 2013, MNRAS, 435, 2835 (W13)

Wyse R. F. G., 2001, in Funes J. G., Corsini E. M., eds, ASP Conf. Ser. Vol. 230. Galaxy Disks and Disk Galaxies. The Merging History of the Milky Way Disk. Astron. Soc. Pac., San Francisco, p. 71

APPENDIX A:

A1 Varying the p_{bar} threshold

As described in the main text, the threshold we choose for p_{bar} is selected so bars in our GZH sample should have similar properties (i.e. strength) to those in the GZ2 low-redshift comparison sample. We allude to the fact that differing bar fractions observed at low and high redshifts may be due to different strengths of bars being used to determine such results. Fig. 11 of W13 illustrates for GZ2 how p_{bar} correlates with the length of bars relative to their disc. Here we explore the redshift evolution of the bar fraction for a range of p_{bar} thresholds (from $p_{bar} \geq 0.3$ to $p_{bar} \geq 0.7$), where we expect a lower threshold to include weak bars, and the higher threshold to only include the 'strongest' bars.

Fig. A1 gives examples of galaxies with a range of p_{bar} and redshift values. Combining these images with those from Fig. 4, which show disc galaxies with $p_{bar} = 0$ and $p_{bar} \sim 1$, we provide images which illustrate the full range of p_{bar} values ($0 \leq p_{bar} \leq 1$) at selected redshift values within our range ($z = 0.4, 0.6, 0.8, 1$).

Fig. A2 shows the evolution of the bar fraction for each of these thresholds. As expected, the bar fractions seen in each lookback bin differ for each threshold, as expected the bar fraction increases as the threshold is lowered. Linear relationships for each of the
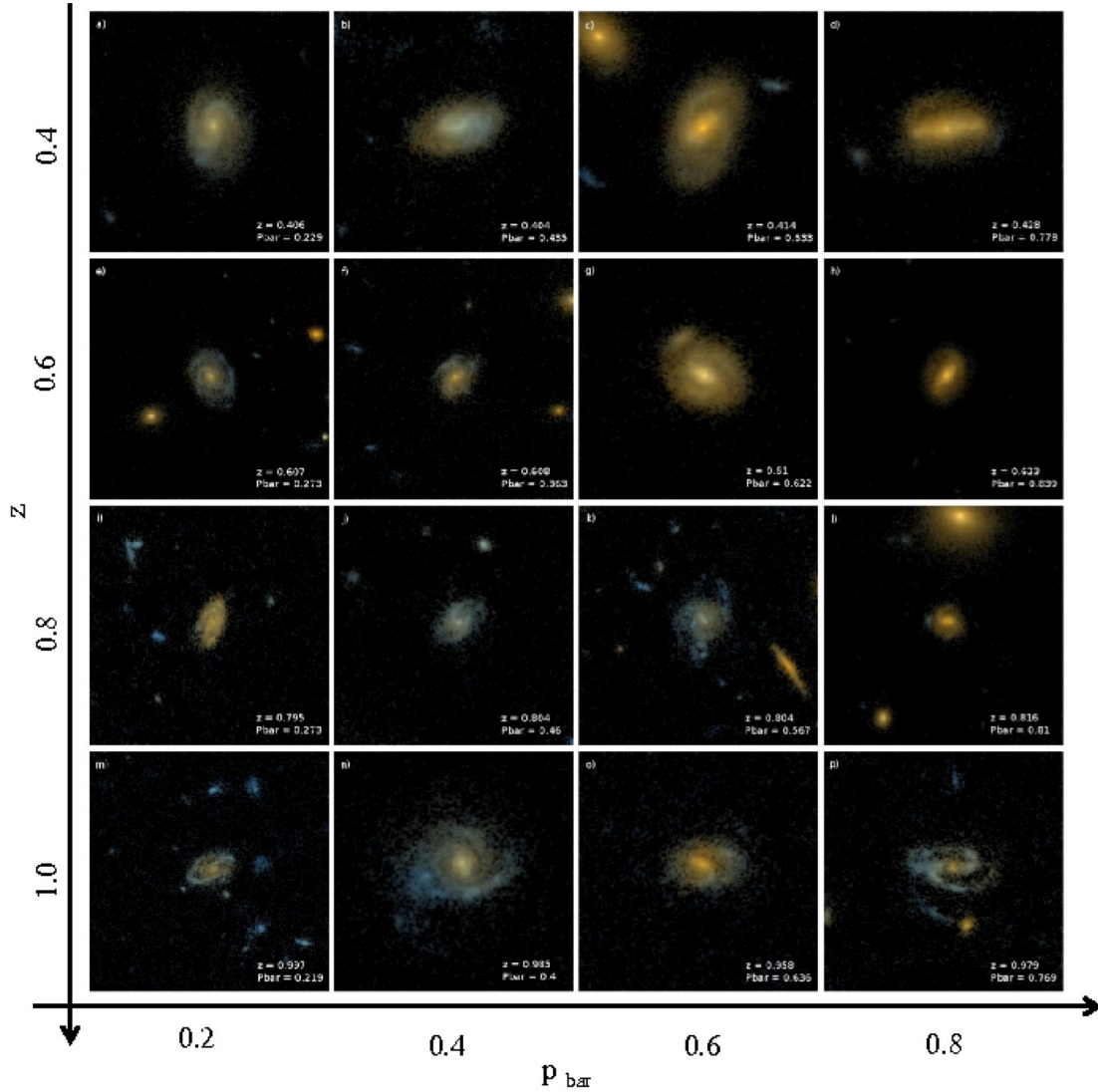
Figure A1. Postage stamp images showing how the strength of a bar is represented by differing p_{bar} values over a range of redshifts. The p_{bar} values increase from left to right, in increments of ~0.2 (i.e. $0.2 \leq p_{bar} \leq 0.8$), with redshift increasing from top to bottom, also in increments of ~0.2 (i.e. $0.4 \leq z \leq 1.0$). Both the redshift and expected weighted likelihood from GZ classifications that the galaxy hosts a barred structure (p_{bar}) are shown in the bottom right hand corner for each image. Fig. 4 shows examples of $p_{bar} = 0$ and $p_{bar} \sim 1$.
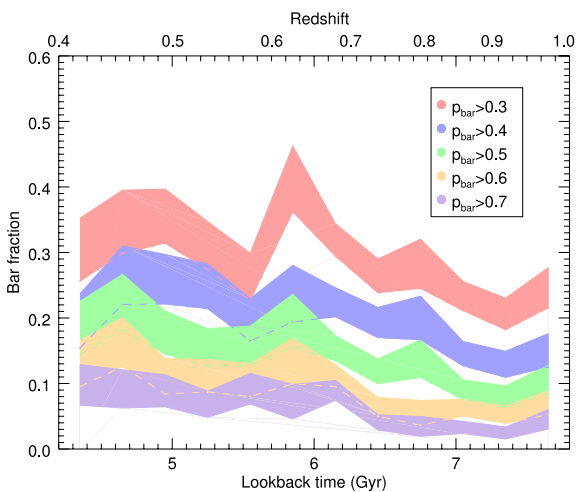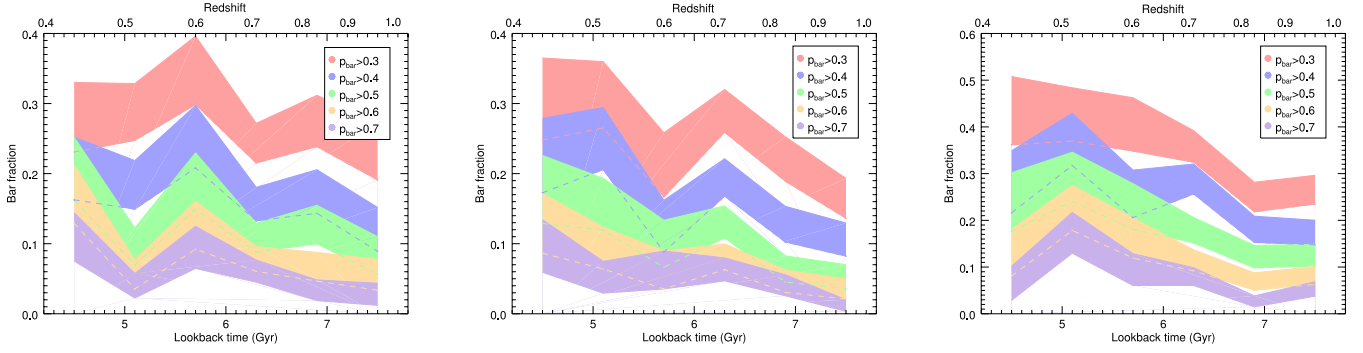

Figure A2. Redshift evolution of the bar fraction for a range of p_{bar} thresholds, with linear relationships for each threshold given in Table A1.

Table A1. Linear equations in the form $f_{bar} = f_{bar, 0} + (\gamma t_{lb}(Gyr))$, which relates the bar fraction evolution to lookback time for differing p_{bar} thresholds.

p_{bar} threshold	$f_{bar, 0}$	γ
≥0.3	0.54 ± 0.06	-0.041 ± 0.010
≥0.4	0.44 ± 0.06	-0.039 ± 0.009
≥0.5	0.38 ± 0.05	-0.039 ± 0.008
≥0.6	0.26 ± 0.04	-0.028 ± 0.006
≥0.7	0.21 ± 0.04	-0.024 ± 0.005

thresholds are shown in Table A1. We show that varying the p_{bar} threshold does not significantly change the slope of the trend seen in our results, where the bar fraction increases towards lower redshifts. We do find that the rate of increase of the bar fraction towards lower redshifts does slightly increase as the p_{bar} threshold is reduced.

In Fig. A3, we explore the mass-dependent redshift evolution of the bar fraction for the p_{bar} thresholds used in Fig. A2. As we

Figure A3. Redshift evolution of the bar fraction for a range of p_{bar} thresholds for each stellar mass range described in Section 2.4. Left: low-mass disc galaxies; Centre: intermediate-mass disc galaxies; Right: high-mass disc galaxies. The linear relationships for the differing p_{bar} thresholds in each mass range are given in Table A2.

Table A2. Linear equations in the form $f_{bar} = f_{bar,\,0} + (\gamma\,t_{lb}(\text{Gyr}))$, which relates the bar fraction evolution to lookback time for differing p_{bar} thresholds for each stellar mass bin: Top: low mass; middle: intermediate mass and bottom: high mass.

p_{bar} threshold	$f_{bar,\,0}$	γ
Low-mass sample – $10.0 \leq \log(M_\star/M_\odot) < 10.34$		
≥ 0.3	0.39 ± 0.11	-0.020 ± 0.017
≥ 0.4	0.34 ± 0.09	-0.027 ± 0.014
≥ 0.5	0.24 ± 0.08	-0.019 ± 0.013
≥ 0.6	0.16 ± 0.07	-0.013 ± 0.010
≥ 0.7	0.14 ± 0.05	-0.015 ± 0.008
Intermediate-mass sample – $10.34 \leq \log(M_\star/M_\odot) < 10.64$		
≥ 0.3	0.55 ± 0.11	-0.049 ± 0.016
≥ 0.4	0.43 ± 0.09	-0.043 ± 0.014
≥ 0.5	0.37 ± 0.08	-0.043 ± 0.012
≥ 0.6	0.23 ± 0.07	-0.027 ± 0.010
≥ 0.7	0.21 ± 0.05	-0.025 ± 0.007
High-mass sample – $\log(M_\star/M_\odot) \geq 10.64$		
≥ 0.3	0.79 ± 0.13	-0.072 ± 0.019
≥ 0.4	0.64 ± 0.11	-0.062 ± 0.017
≥ 0.5	0.53 ± 0.11	-0.056 ± 0.016
≥ 0.6	0.35 ± 0.09	-0.037 ± 0.013
≥ 0.7	0.22 ± 0.07	-0.024 ± 0.010

found for the GZH sample as a whole, the absolute bar fractions observed in each of the stellar mass ranges increase as the p_{bar} threshold drops. The rate of increase of the bar fraction with time, shown in Table A2, also becomes steeper as p_{bar} is reduced. Despite these differences, the observed trends we discussed in Section 4.2 remain for all p_{bar} thresholds, across each of the three stellar mass bins.

This paper has been typeset from a TeX/LaTeX file prepared by the author.